On the ability to exploit signal fluctuations in pseudocontinuous Arterial Spin Labeling for inferring the major flow territories from a traditional perfusion scan

Harten, T.W. van; Dzyubachyk, O.; Bokkers, R.P.H.; Wermer, M.J.H.; Osch, M.J.P. van

NeuroImage 230 (2021) 117813

Contents lists available at ScienceDirect

NeuroImage

journal homepage: www.elsevier.com/locate/neuroimage

On the ability to exploit signal fluctuations in pseudocontinuous arterial spin labeling for inferring the major flow territories from a traditional perfusion scan

T.W. van Harten[a,*], O. Dzyubachyk[b], R.P.H. Bokkers[c], M.J.H. Wermer[d], M.J.P. van Osch[a]

[a] C.J. Gorter Center for High Field MRI, Department of Radiology, Leiden University Medical Center, Postbus 9600, 2300 RC Leiden, the Netherlands
[b] Division of Image Processing (LKEB), Department of Radiology, Leiden University Medical Center, Postbus 9600, 2300 RC Leiden, the Netherlands
[c] Department of Radiology, Medical Imaging Center, University Medical Center Groningen, University of Groningen, Postbus 30.001, 3700 RB Groningen, the Netherlands
[d] Department of Neurology, Leiden University Medical Center, Postbus 9600, 2300 RC Leiden, the Netherlands

ARTICLE INFO

Keywords:
Arterial spin labeling
Flow territories
Postprocessing
Off-resonance effects

ABSTRACT

In arterial spin labeling (ASL) a magnetic label is applied to the flowing blood in feeding arteries allowing depiction of cerebral perfusion maps. The labeling efficiency depends, however, on blood velocity and local field inhomogeneities and is, therefore, not constant over time. In this work, we investigate the ability of statistical methods used in functional connectivity research to infer flow territory information from traditional pseudo-continuous ASL (pCASL) scans by exploiting artery-specific signal fluctuations. By applying an additional gradient during labeling the minimum amount of signal fluctuation that allows discrimination of the main flow territories is determined. The following three approaches were tested for their performance on inferring the large vessel flow territories of the brain: a general linear model (GLM), an independent component analysis (ICA) and t-stochastic neighbor embedding. Furthermore, to investigate the effect of large vessel pathology, standard ASL scans of three patients with a unilateral stenosis (>70%) of one of the internal carotid arteries were retrospectively analyzed using ICA and t-SNE. Our results suggest that the amount of natural-occurring variation in labeling efficiency is insufficient to determine large vessel flow territories. When applying additional vessel-encoded gradients these methods are able to distinguish flow territories from one another, but this would result in approximately 8.5% lower perfusion signal and thus also a reduction in SNR of the same magnitude.

1. Introduction

pCASL is a readily available non-invasive technique for perfusion imaging that can be used in a clinical setting (Alsop et al., 2015), for clinical research, as well as for neuroscience applications, such as identification of neuronal networks (Dai et al., 2016). By applying vessel encoding, pCASL can also be used to infer flow territories of arteries (Gevers et al., 2012; Wong, 2007; Wong and Guo, 2012). Whereas current clinical practice relies on general atlases of typical flow territories, information on the layout of the actual flow territories in an individual patient can be highly valuable in several clinical settings, such as for risk assessment and guidance of revascularization therapy in patients suffering from stroke, as well as for explaining differences in patient outcome (Hartkamp et al., 2016; Hendrikse et al., 2009; van Laar et al., 2008).

Small changes in ASL signal over time allow for identification of resting state networks (Dai et al., 2016). One could hypothesize that small, artery specific signal fluctuations in pCASL-signal would allow to also infer the flow territories from a traditional perfusion scan. Such signal changes could both arise from physiological fluctuations within a flow territory, as well as from the acquisition process. For example, the labeling efficiency of pCASL is known to be dependent on velocity of arterial blood and off-resonance effects at the labeling location (Aslan et al., 2010; Wu et al., 2011, 2007). Any variation in labeling efficiency of a particular artery will affect the ASL-signal of the complete associated flow territory, and, differences between arteries could therefore provide a source of flow-territory-specific signal fluctuations that could be exploited for identifying these territories. Similarly, dynamic changes in arterial transport times could also induce flow-territory-specific fluctuations. (Qiu et al., 2010; Verbree and van Osch, 2018) This could be a way of acquiring flow territory information for free from a 2D-multi-slice pCASL scan, which normally has many (>25) repeated measurements. When natural occurring fluctuations would be sufficient, this would enable a penalty-free approach for obtaining combined cerebral blood flow (CBF) and flow territory information from a single scan. Alternatively, small labeling-efficiency fluctuations could be inserted into the sequence, which would only result in a minor SNR penalty on the perfusion scan. To assess the feasibility of such an approach, we analyzed ASL scans by several techniques traditionally used in functional connectivity

* Corresponding author.
E-mail address: T.W.van_Harten@lumc.nl (T.W. van Harten).

https://doi.org/10.1016/j.neuroimage.2021.117813
Received 27 July 2020; Received in revised form 14 January 2021; Accepted 20 January 2021
Available online 29 January 2021

research. Moreover, by incorporating different levels of signal fluctuations into pCASL scans, it was determined what level of signal variations is needed to allow assessment of flow territory information. Vessel-encoded signal fluctuations were introduced by deliberately changing the labeling efficiency of the left and right internal carotid artery by adding a vessel-encoding gradient (Gevers et al., 2012; Wong, 2007) with variable strength into a normal pCASL sequence. The three methods tested are already commonly used in functional MRI analyses: 1) general linear model (GLM) based approach, as generally used in task based fMRI (Yerys et al., 2018); The GLM based approach was selected to represent the best-case scenario: by including the timing of the inserted signal fluctuations into the analysis an upper-limit of performance of flow-territory extraction can be established. 2) Independent component analysis (ICA), as generally used in resting state fMRI (Dai et al., 2016); and 3) t-stochastic neighbor embedding (t-SNE), a clustering method with broad applications in image processing (Hu et al., 2020). ICA and t-SNE are input naïve approaches as they do not rely on the knowledge of the timing of signal fluctuations and could, therefore, also be used for traditional pCASL data when no additional signal fluctuations are inserted. The ICA was performed both on the original data, as well as on the data after blurring with a 10 mm kernel. The addition of the 10 mm blurred version was based on the hypothesis that the relatively low SNR of single average ASL images would hamper identification of flow territory specific fluctuations. Since such fluctuations would per definition be spatially coherent, some blurring could help in identifying flow territories, albeit at a loss of effective spatial resolution.

Finally, to investigate this approach in patient cases, we retrospectively analyzed pCASL scans of patients with an internal carotid stenosis and compared the outcome with the flow territories obtained from a separately acquired vessel-encoded pCASL scan. In this proof-of-concept study only the flow territories of the right and left internal carotid artery were considered.

2. Methods

pCASL scans with different levels of vessel-encoded signal fluctuations were acquired in 5 volunteers with traditional flow territory scans obtained as ground truth. The scans were subsequently analyzed using three different statistical methods: a general linear model (GLM), an independent component analysis (ICA), and a t-Stochastic neighbor embedding (t-SNE) approach. The FMRIB's Software Library (FSL, www.fmrib.ox.ac.uk/fsl) was used for the GLM and ICA approaches, while the t-SNE was performed using an inhouse developed pipeline, as further described in *Applied Models*. The pCASL scans acquired without a vessel-encoding gradient were analyzed only using the ICA and t-SNE methods, since the GLM-approach relies on prior knowledge on the timing of the fluctuations in labeling efficiency, which is not available when there is no prior knowledge on the pattern of signal fluctuations.

2.1. Participants

This research has been performed in accordance with the declaration of Helsinki. Written informed consent was obtained from all participants. Five healthy participants (mean age 30.4 ± 7.6, male/female = 4/1) were recruited for this study. Since one might expect that patients show larger natural occurring fluctuations than healthy participants, data from three patients (mean age: 69.7 ± 9.5, male/female = 2/1) with a recently symptomatic unilateral internal carotid stenosis (>50% occluded) were retrospectively analyzed.

2.2. Scans

All healthy participants were scanned on a 3 T MRI scanner (Achieva, Philips Medical Systems, the Netherlands) using a protocol containing a standard background suppressed pCASL (TR/TE 4290/16 ms, FOV $240 \times 240 \times 119$ mm^3 matrix size 80×80, 17 slices with no interslice gap resulting in a voxel-size of $3 \times 3 \times 7$ mm^3, labeling duration = 1800 ms, post-labeling delay (PLD) of 1800 ms with 35 repetitions resulting in a total scan duration of 5 min 09 s), a time-of-flight angiogram of the labeling plane (TR/TE 35/3.5 ms, flip angle 60°, 9 slices with a slice thickness of 3 mm, FOV $230 \times 230 \times 19$ mm^3, matrix size 192×96, resulting in a pixel-size of 1.2×2.4 mm^2 and a scan duration of 31 s), a vessel-encoded flow territory mapping scan, considered as the gold standard, with similar settings as the standard pCASL scan, but acquired in 5 conditions: 1) label, 2) control, 3) vessel-encoding in the RL direction with a distance of 50 mm between full label and control, 4) and 5) two vessel-encodings in the AP direction with a distance of 15 mm with the last condition shifted 7.5 mm compared to the first (Gevers et al., 2012) (12 averages, resulting in a scan duration of 4 min 39 s) The vessel encoding distance is defined as the distance between the location where optimal labeling occurs (always planned to be on top of an internal carotid artery) and the location where the control condition is achieved, an equivalent definition is the distance over which a pi phase will occur due to the vessel encoding gradient. E.g. a vessel encoding distance of 50mm (average distance between internal carotid arteries) would have the targeted internal carotid artery in label condition while the contralateral artery would we in control condition. The protocol also included a range of pCASL scans with an additional vessel-selective gradient in the left-right direction with varying gradient strengths according to a predefined scheme (see Fig. 1), whose scan parameters were otherwise identical to the standard pCASL scan. The varying gradient strength values were chosen to create artery-specific signal fluctuations by having maximal labeling efficiency at the location of one internal carotid artery, while the contralateral internal carotid artery will experience sub-optimal labeling. The phases of the pCASL labeling pulses were adapted to ensure that the optimal labeling condition was achieved on top of one of the internal carotid arteries. By changing the area under the vessel-encoding gradient by adjusting its amplitude, the spatial frequency of the induced label efficiency changes in the direction of the vessel-encoding gradient can be controlled. With optimal labeling in one internal carotid artery, the contralateral internal carotid artery will experience off-resonance effects and thus a lower labeling efficiency. The magnitude of the off-resonance effects will determine the extent of the labeling efficiency decrease. The term "vessel-encoding distance" will be used for the distance resulting in π phase shift during the interpulse interval of the pCASL train. At this distance from the internal carotid artery with optimal labeling, the control and label condition will be switched compared to the targeted vessel.

The position of optimal labeling is switched to the contralateral internal carotid artery after acquisition of each label control pair, resulting in a switch in signal intensity of the flow territories after every label/control pair. This was done in order to create temporal fluctuations in labeling efficiency for both internal carotid arteries, while providing a normal perfusion map when averaging all data, albeit with lower mean labeling efficiency.

The data from patients with a unilateral internal carotid artery stenosis was acquired as part of a previously published study. (Hartkamp et al., 2011) All patients had suffered a transient ischemic attack (TIA) or non-disabling ischemic stroke ipsilateral to the internal carotid artery stenosis. The protocol included standard pCASL (TR/TE 4000/14 ms, FOV 240×140 mm^2, matrix size 89×79, 17 slices with no interslice gap resulting in a voxel-size of $3 \times 3 \times 7$ mm^3, labeling duration = 1650 ms, post-labeling delay (PLD) of 1525 ms with 38 repetitions resulting in a total scan duration of 5 min 26 s), and a planning-free flow territory mapping scan with the same settings.

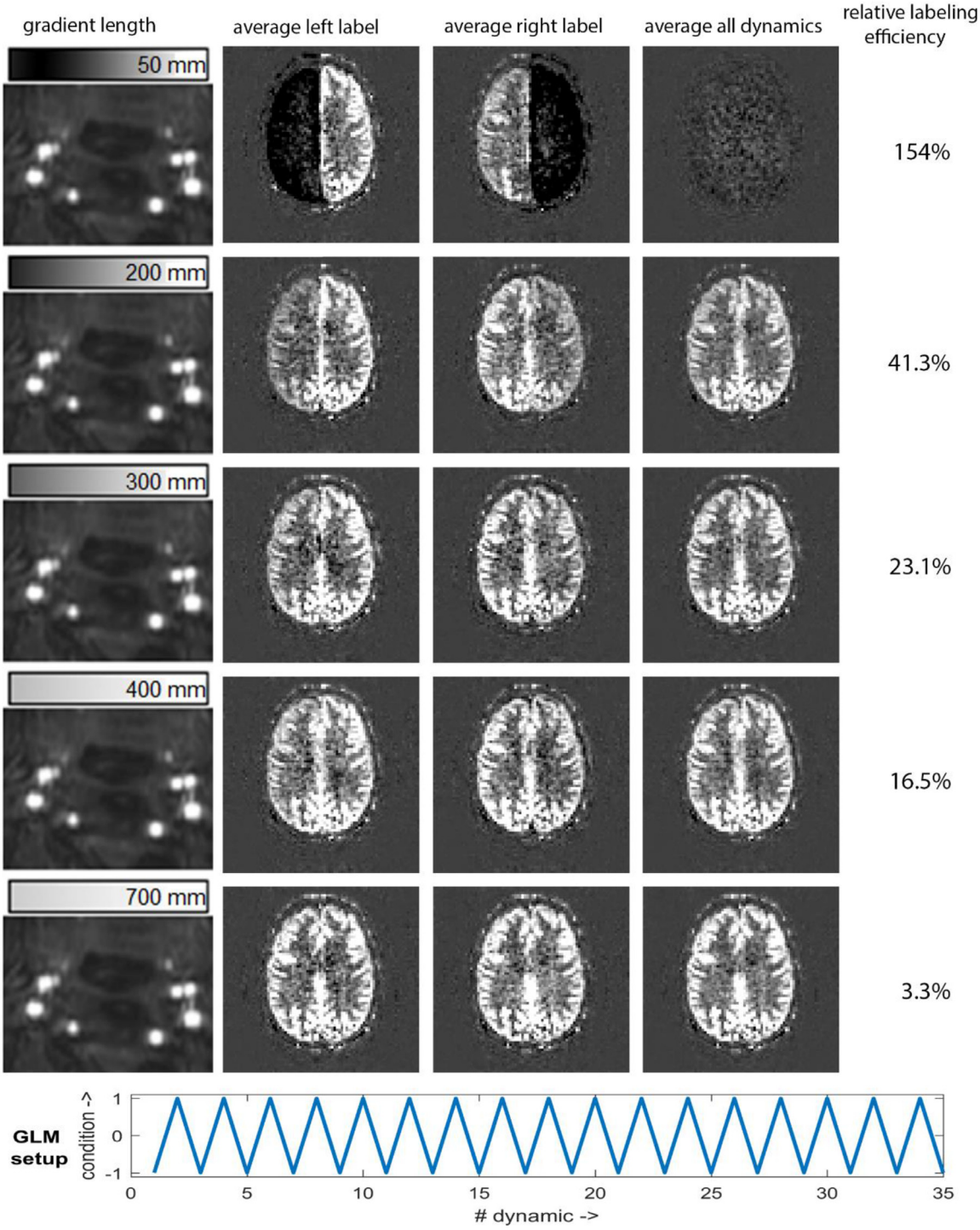

Fig. 1. The effect of the area of the vessel-encoding gradient on the ASL-signal in an example subject; with amplitude of the vessel-encoding gradient varying from strong (top) to weak (bottom). The first column shows Time-Of-Flight angiography of the labeling plane with the bar above indicating how the vessel-encoding gradient affects the labeling efficiency: white is optimal labeling and black the location where an additional π phase shift occurs during the pulse-interval, which will result into opposite behavior during labeling (i.e. control during the label, and label during the control condition). The numbers reflect the vessel-encoding distance. Since optimal labeling is switched between the left to the right internal carotid artery after every label-control pair, the data were split into two. Columns two and three show the resulting mean ASL subtraction image when the left or right internal carotid artery was labeled optimally. The final column shows the mean signal intensity over the complete pCASL scans, i.e. the average of the second and third column, showing a homogenous image, except for the first row that shows signal cancelations. The percentages on the right indicate the relative signal fluctuations for the images shown in this figure, as calculated by Eq. (1). The bottom row shows the design for GLM setup.

2.3. Post-processing

First, the flow territories of both internal carotid arteries and the basilar artery were determined by processing vessel-encoded flow territory mapping scans, using previously described methods (Gevers et al., 2012).The effect of the applied vessel-encoding gradient on the labeling efficiency was quantified for each flow territory as the mean signal intensity after subtracting and averaging the images with suboptimal conditions due to the presence of the vessel-encoding gradient ($SI_{off\text{-}resonance}$) from the images with the artery in perfect labeling condition (SI_{full}); and subsequently normalizing by the mean signal intensity as measured by the standard pCASL scan (SI_{pCASL}):

$$\text{Relative signal fluctuations} = \left(SI_{full} - SI_{off\text{-}resonance}\right)/SI_{pCASL} * 100\% \quad (1)$$

2.3. Applied models

Four different approaches were selected to extract the flow territories based upon flow-territory-specific signal fluctuations.

Data preprocessing for the GLM and ICA based methods was performed using FSL (FMRIB's Software Library, www.fmrib.ox.ac.uk/fsl). The following preprocessing was applied: motion correction using MCFLIRT; non-brain removal using BET (Smith, 2002); grand-mean intensity normalization of the entire 4D dataset by a single multiplicative factor; high-pass temporal filtering (Gaussian-weighted least-squares straight line fitting, with sigma=50.0 s for both GLM and ICA).

2.3.1. General linear model

In the GLM the applied labeling fluctuations were introduced into the model as an explanatory variable. Because the multiple regression of the GLM requires such prior information, it is not possible to do this analysis on scans where no intentional signal fluctuations were inserted by means of additional gradients switched on in the labeling plane. The general linear model was carried out using FEAT (FMRI Expert Analysis Tool) Version 6.00, part of FSL (FMRIB's Software Library, www.fmrib.ox.ac.uk/fsl). The time-series statistical analysis was carried out using FILM with local autocorrelation correction. Only lower level analysis was applied as this was ran on a single 4-D MRI experiment. *T*-statistic maps resulting from this analysis were used without thresholding or clustering.

2.3.2. Independent component analysis

ICA analysis was carried out using Probabilistic Independent Component Analysis implemented in MELODIC (Multivariate Exploratory Linear Decomposition into Independent Components) Version 3.15, part of FSL. In summary, pre-processed data were whitened and projected into a multi-dimensional subspace using a probabilistic Principal Component Analysis where the number of dimensions was estimated using the Laplace approximation to the Bayesian evidence of the model order (Beckmann et al., 2001; Minka, 2000). The whitened observations were subsequently decomposed into sets of vectors that describe signal variation across the temporal domain (time-courses) and across the spatial domain (maps) by optimizing for non-Gaussian spatial source distributions using a fixed-point iteration technique (Hyvarinen, 1999). Estimated component maps were divided by the standard deviation of the residual noise and thresholded by fitting a mixture model to the histogram of intensity values (Beckmann and Smith, 2004). From the identified components, the best fitting was selected based upon the largest difference between left and right intracranial region defined by a left and right hemisphere mask containing intracranial voxels separated by a (mid-)sagittal plane crossing through the genu and splenum of the corpus callosum. The component with the highest corroboration with the corresponding hemisphere mask was used as outcome for that flow territory for further evaluation.

Finally, the complete MELODIC was repeated after blurring the input data with a 10 mm Gaussian kernel to minimize the effect of voxel-level inconsistencies.

2.3.3. t-Distributed stochastic neighbor embedding

Since we are only interested in differentiating left and right flow-territories, which is effectively a 1D problem, we set the target embedding dimensionality to unity. The ASL difference volumes were reduced in the time dimension to a single value by applying the Hierarchical Stochastic Neighbor Embedding (HSNE) algorithm (Pezzotti et al., 2016). HSNE is a modification of the classical t-SNE algorithm, which was proven to better preserve the data structure during the embedding process (van der Maaten and Hinton, 2008). Full embedding of each of the data sets was performed as a hierarchical process with 4 levels. Drilling down into the next level of the hierarchy was performed after convergence (defined as the maximum number of iterations) of the embedding on the current level. All the landmarks available on the current level were used for this. Initial positions of the lower-level landmarks were calculated by interpolating current positions of the corresponding higher-level landmarks.

2.4. Validation

The robustness of the methods was tested via receiver operating characteristic (ROC) curves, only including intracranial voxels that show sufficient ASL-signal. Moreover, since signal fluctuations were only introduced in the internal carotid arteries, voxels that are part of the posterior circulation territory as determined from the flow territory maps were excluded. Sufficient ASL-signal was operationalized, as the lower limit of values within the gray matter, which was determined via a consensus value over all participants and was kept constant for all scans. Voxels with lower signal, such as those in the white matter, were excluded from the analysis, because they could not be classified on the flow territory mapping data and are, therefore, not a correct reflection of the performance of the different approaches, and would introduce bias in the evaluation procedure.

The *z*-statistics map of the GLM-based approach, the IC-map of the ICA-based approaches, as well as the distance maps from the t-SNE-based approach were projected on the ground truth flow territory maps. ROC curves were generated by thresholding the statistical maps reflecting the z-score/distance to yield binary segmentations and subsequently calculating the overlap with the flow territory map. This analysis was done with an in-house developed pipeline combining MeVisLab 3.2 and Matlab 2016a.

3. Results

The vessel-encoding gradients we introduced did lead to the intended changes in ASL signal fluctuation. These fluctuations were directly proportional to the gradient area of the employed vessel-encoding gradients. In *Fig. 1* the effect of vessel-encoding gradient-area on the ASL-images is shown for one subject. For displaying the magnitude of the induced signal fluctuations, the ASL-scans were split into those measurements for which the left internal carotid artery was optimally labeled and those that targeted the right internal carotid artery. From these images we can conclude that the proposed approach indeed leads to a tunable magnitude of labeling efficiency fluctuations on top of a normal ASL-scan. The chosen strength values for the vessel-encoding lead to fluctuations between 3% and 150%.

The averaged effect over all participants of the area under the vessel-encoding gradient on the relative signal fluctuations is shown in *Fig. 2*, showcasing the direct relationship between the introduced off-resonance effects in the labeling plane and ASL-signal fluctuations downstream within the flow territories of these arteries. The smaller the area under the vessel-encoding gradient, the smaller the off-resonance effects in the contralateral internal carotid artery, and the smaller the difference in relative signal fluctuations between the two flow territories of these arteries.

Fig. 3 shows how well the four different post-processing approaches could detect the underlying flow territories for a single example subject

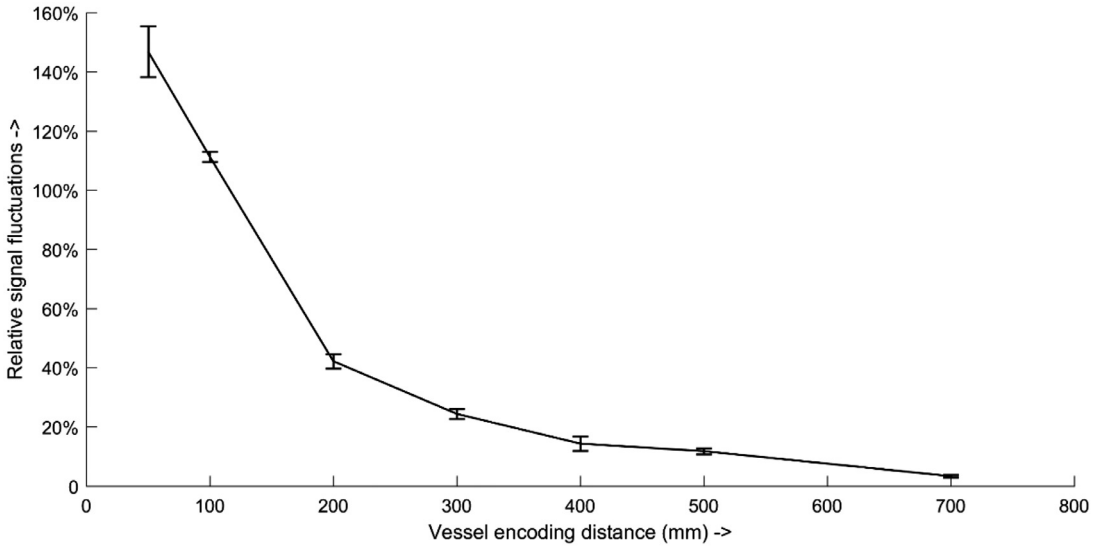

Fig. 2. Mean relative signal fluctuations as a function of vessel-encoding distance; (distance resulting in π phase shift during the interpulse interval of the pCASL train) with standard error of the mean for all participants.

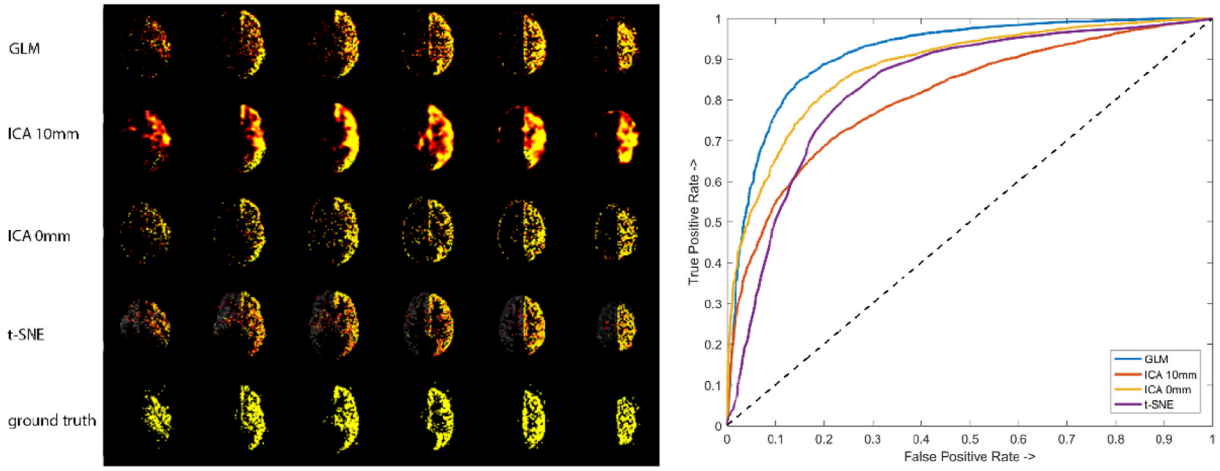

Fig. 3. Post-processing approaches and their ability to detect flow territories; example of how well the four post-processing approaches can detect the flow territories on the data from the second row of Fig. 1, i.e. a vessel-encoding distance of 200 mm, corresponding to a relative signal fluctuation of 41.3%. From top to bottom: GLM, ICA with 10 mm blurring, ICA without blurring, t-SNE, and flow territory mapping. In the right panel, the ROC are shown for the same data. The dashed line indicates a hypothetical 50/50 random chance classifier.

(same subject as *Fig. 1*). It can be seen that, as the strength of the vessel-encoding gradient is strong enough, all 3 methods can identify the flow territory correctly, but specificity and sensitivity vary between the four approaches, which is also reflected in the ROC curves displayed on the right.

Fig. 4 summarizes the mean and standard deviation of the area under the ROC curves over all 5 participants, over all labeling conditions. The averages of the area under the curve of the ROC curves show that the GLM-based approach does outperform the other methods in this dataset, which was expected because the GLM exploits prior knowledge of the applied labeling fluctuations. In the scans with the strongest signal fluctuations the ICA was found to split flow territories in multiple components. Only the component with the strongest difference between left and right was used in further analyses. Furthermore, for most levels of relative signal fluctuations, blurring improved the ability of the ICA-based approach to differentiate between flow territories, although this was not the case for all participants or for all conditions. When the differences in fluctuations were especially large (>200 mm gradient length) or small (<500 mm gradient length), there was an agreement between the blurring and non-blurring results, while for conditions between these two extremes, better results were obtained when blurring the input data.

The ICA as well as the t-SNE analysis on the pCASL data without imputed signal fluctuations did not yield convincing flow territory information, in either healthy volunteers nor the patients with internal carotid artery stenosis (Fig. 5).

4. Discussion

The main findings of this study are threefold. First, we are able to report that with the introduction of weak off-resonance effects by means of a vessel-encoding gradient it becomes possible to determine flow territories using a GLM statistical analysis. The performance becomes weaker in robustness when the introduced fluctuations are smaller or when “naive methods” are employed, i.e. when no prior information on the timing of the labeling efficiency fluctuations is exploited in the statistical model. We observe a statistically significant higher ROC for GLM, but this should be interpreted with care due to the very small sample size of our study Second, when maintaining a minimum of 0.85 for the

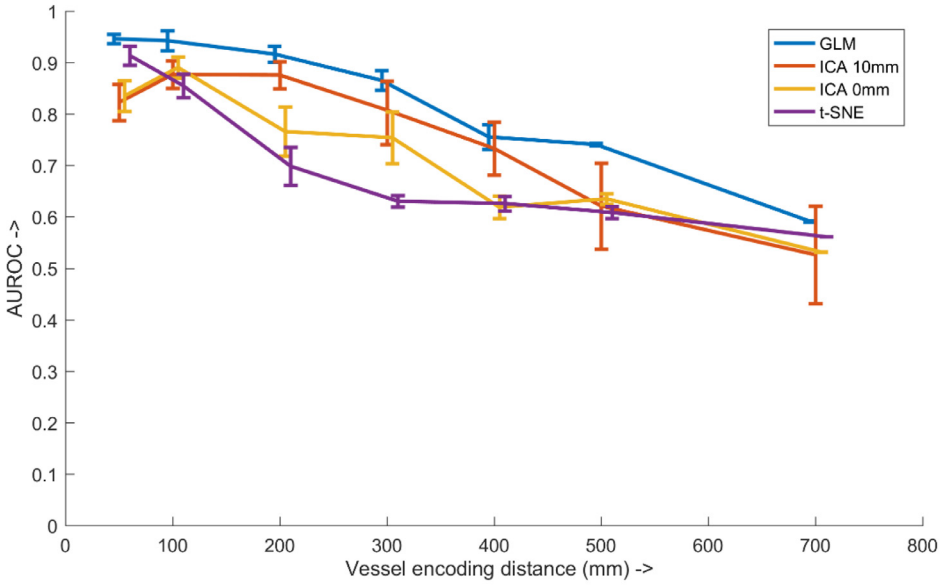

Fig. 4. Mean area under the ROC-curve for each method as a function of the vessel encoding distance; error-bars indicate standard error of the mean. A small offset in the *x*-direction was introduced for each method for illustration purposes.

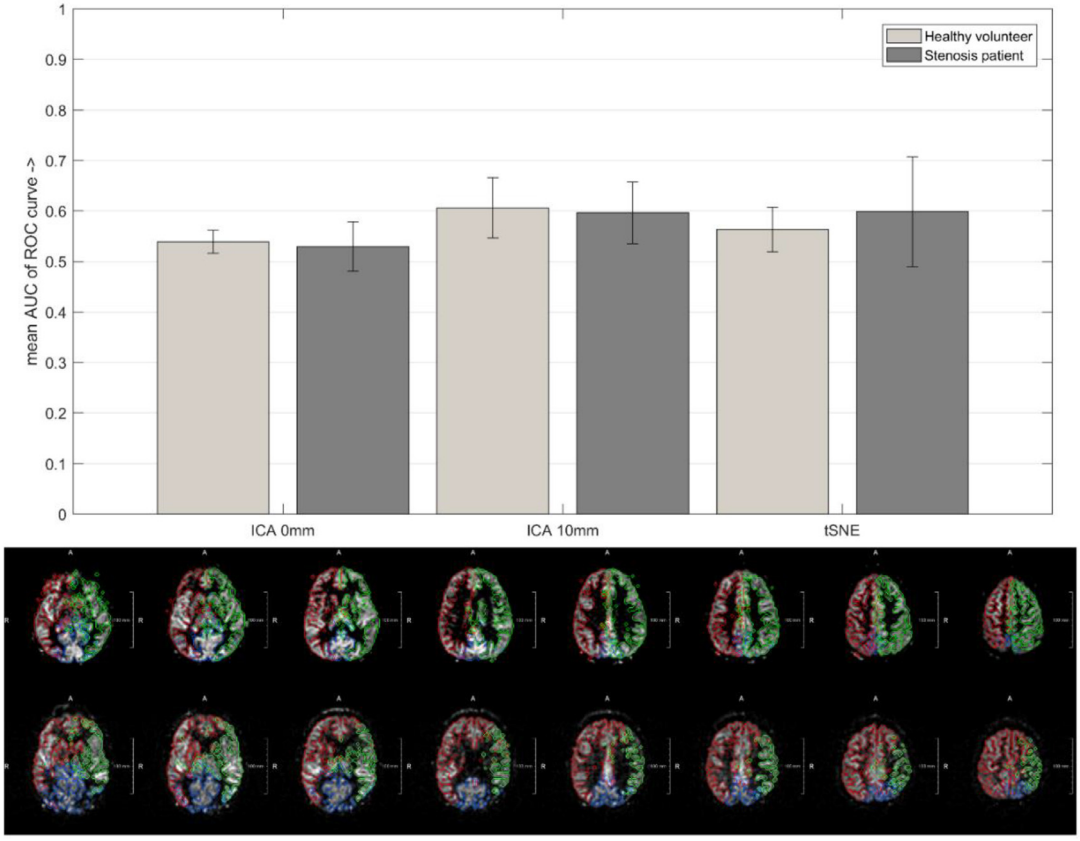

Fig. 5. Mean area under the ROC-curve for each method tested on standard pCASL scans; all methods were slightly better than a 50/50 chance classifier but unable to determine flow territories. There was no significant difference between healthy volunteers and patients with a unilateral stenosis in the internal carotid artery. Error bars indicate standard error of the mean.

area under the ROC-curve to reflect correct performance, the ICA and t-SNE approaches lost their ability to differentiate between left and right flow territory at a relative signal fluctuations of 41.3% and 64.1%, respectively. Third, it was not feasible to determine reliable flow territory information from traditional pCASL scans in healthy volunteers or patients with >70% unilateral carotid stenosis using ICA or t-SNE analysis, i.e. natural occurring fluctuations in labeling efficiency in the temporal domain were insufficient to yield reliable flow territory information.

Coherent fluctuations within a flow territory were found to be too small to identify them from conventional pCASL scans, whereas fluctuations caused by hemodynamic fluctuations were previously found to allow detection of resting state networks, albeit at group level (Dai et al., 2016). This can be considered a surprising finding: coherent hemo-

dynamic fluctuations as observed in resting-state fMRI/ASL have a more substantial influence than any flow-territory specific hemodynamic changes or off-resonance effects. Correct performance of our applied post-processing methodology was proven by showing that imputed labeling efficiency fluctuations did allow differentiation between the left and right internal carotid artery territory. One explanation might be that fluctuations in labeling efficiency are mainly caused by global systemic processes. For example, heart rate or respiratory variations will affect all brain-feedings arteries territories similarly, just as fluctuations in end-tidal CO_2 will have a global rather than an artery specific effect. The impact of breathing on the labeling efficiency can be estimated from previously reported resonance frequency changes (Raj et al., 2001; Versluis et al., 2012). For example, Birn et al. (1998) and Zhao et al. (2017) showed that off-resonance frequencies during swallowing and speech reach up to −9.6 Hz at 3 T in the inferior part of the brain, which would result in a phase shift of 4.14° during the 1.2 ms between the pCASL pulses, i.e. a rather limited effect although the effect at the labeling plane could be expected to be a bit more pronounced.

When 16.5% or stronger fluctuations of ASL-signal were imputed on the perfusion signal, reliable discrimination between the right and left internal carotid artery flow territory could be achieved by using the GLM approach. These fluctuations are larger than the fluctuations described earlier induced by respiration and other physiology (Birn et al., 1998; Zhao et al., 2017). The presence of such a gradient implies that the mean labeling efficiency will be 8.3% lower over the whole ASL-acquisition (labeling is only decreased in half of the measurements), which translates directly to 8.3% lower SNR of the perfusion map when compared to an ASL scan with the same scan time. This seems to be on the border of what could be considered acceptable in a clinical setting to allow combined flow territory and perfusion imaging. Also, slight interindividual differences in location of the arteries could affect the induced labeling efficiency reduction between the left and right internal carotid artery, when relying on population averaged settings for the planning of the location of perfect labeling conditions. This would imply that the average perfusion map could become asymmetrical, which might affect clinical interpretation, although also in normal pCASL scans labeling efficiency differences between arteries have been reported (Chen et al., 2018).

Other approaches for improving vessel encoded scans involve applying novel acquisition techniques, such as a different labeling scheme to reduce scan time while maintaining sufficient SNR for reliable flow territory determination (Gunther, 2006; Zimine et al., 2006); and approaches to calculate optimal labeling schemes to further improve SNR (Berry et al., 2015). These approaches, however, require specific planning approaches and may therefore introduce differences in performance between technicians. Furthermore, these approaches would not be able to extract any additional flow territory information from traditional pCASL scans.

In this study, four different post-processing approaches were tested in their ability to determine flow territory information from small fluctuations in labeling efficiency in the feeding arteries. Based on observed trends in data of this study the most robust method appears to be a GLM-based approach. This is caused by the prior information that is fed into the model, thereby increasing the statistical power of the model. The relative performance of the naïve methods seems at first glance more difficult to describe, since t-SNE outperforms both ICA-based methods on the biggest and the smallest amount of signal fluctuations, whereas in-between the ICA-based approaches perform better. However, for the strongest signal fluctuations, the ICA was found to split flow territories in multiple components, whereas for the validation only a single component was included. This explains the poorer performance of the ICA-methods for the data with the largest signal fluctuations.

We hypothesized that patients with large vessel disease could show more prominent differences in ASL-signal fluctuations between flow territories than healthy volunteers. However, in the three patients that we included in this study, the ICA and t-SNE analyses did not allow trustworthy determination of the flow territories. Apparently, also in carotid stenotic disease patients, fluctuations in ASL-signal are too correlated between flow territories or, in general, too small to allow differentiation.

A limitation of our experimental approach is that we only focused on differentiation between the left and right internal carotid artery territory and ignored the posterior circulation. This approach was taken for practical reasons: we aimed at primarily demonstrating the possibilities for the main internal carotid artery territories and would expand our efforts to the three regions when successful. Moreover, the distance between the two internal carotid arteries is larger than the distance between the anterior and posterior circulation, which could result in larger difference in fluctuations caused by off-resonance effects, i.e. in data without additional vessel-encoding gradients. To be able to discriminate the posterior from the anterior circulation, stronger gradients should be employed than used in the current studies, since the distance between arteries is smaller. Discrimination of vessels distanced more than 5 mm could be achieved, although planning the location of optimal labeling would require an angiographic scout and careful planning In the data without additional flow-encoding gradients, we also tried to discriminate the anterior from the posterior circulation, but this did not provide satisfactory results by either ICA or t-SNE analysis of the ASL-data. Apparently, the difference in hemodynamics between the anterior and posterior circulation does not translate to flow-territory specific fluctuations of the ASL-signal over different repeated measurements.

5. Conclusions

Signal fluctuations present in standard pCASL scans due to fluctuations in off resonance effects in the labeling plane or transit time are not sufficient for extracting flow territory mapping information from standard pCASL scans when using ICA or t-SNE, neither in healthy participants nor in patients with severe (>70%) unilateral internal carotid artery stenosis. When applying additional vessel-encoded gradients these methods are able to distinguish flow territories from one another, but this would result in approximately 8.5% lower perfusion signal and thus also a reduction in SNR of the same magnitude.

Acknowledgments

The authors would like to thank Sophie Schmidt, Wouter Teeuwisse and Annemarieke van Opstal for their help acquiring scan data.

Funding

This research has been made possible by the Dutch Heart Foundation and the Netherlands Organisation for Scientific Research (NWO), as part of their joint strategic research programme: "Earlier recognition of cardiovascular diseases". This project is partially financed by the PPP Allowance made available by Top Sector Life Sciences & Health to the Dutch Heart foundation to stimulate public-private partnerships. This research was also supported by the EU under the Horizon2020 program (project: CDS-QUAMRI), and the CAVIA project (nr. 733050202), which has been made possible by ZonMW

Authorship statement

T.W. van Harten – conceptualization, formal analysis, investigation, writing -original draft.

O. Dzyubachyk – methodology, formal analysis, writing – review & editing.

R.P.H. Bokkers – investigation, writing – review & editing.

M.J.H. Wermer – writing – review & editing, supervision.

M.J.P. van Osch – conceptualization, methodology, writing – review & editing, supervision.

Disclosure of interests

T.W. van Harten – nothing to disclose.
O. Dzyubachyk – nothing to disclose.
R.P.H. Bokkers – nothing to disclose.
M.J.H. Wermer – receives a personal ZonMw grant VIDI (91717337) and Dekker grant, the Netherlands Heart Foundation 2016T086.
M.J.P. van Osch – receives research support from Philips.

Data and code availability statement

The data used in this project is confidential, but may be obtained upon request after signing a data use agreement. Researchers interested in access to the data may contact the last author (M.J.P. van Osch). Prior to sharing the data will be anonymized and scans stripped of all identifiable information, including facial features.

References

Alsop, D.C., Detre, J.A., Golay, X., Gunther, M., Hendrikse, J., Hernandez-Garcia, L., Lu, H., MacIntosh, B.J., Parkes, L.M., Smits, M., van Osch, M.J., Wang, D.J., Wong, E.C., Zaharchuk, G., 2015. Recommended implementation of arterial spin-labeled perfusion MRI for clinical applications: a consensus of the ISMRM perfusion study group and the European consortium for ASL in dementia. Magn. Reson. Med. 73, 102–116.

Aslan, S., Xu, F., Wang, P.L., Uh, J., Yezhuvath, U.S., van Osch, M., Lu, H., 2010. Estimation of labeling efficiency in pseudocontinuous arterial spin labeling. Magn. Reson. Med. 63, 765–771.

Beckmann, C., Noble, J., Smith, S., 2001. Investigating the Intrinsic Dimensionality of FMRI Data for ICA. pp. S76-S76.

Beckmann, C.F., Smith, S.M., 2004. Probabilistic independent component analysis for functional magnetic resonance imaging. IEEE Trans. Med. Imaging 23, 137–152.

Berry, E.S., Jezzard, P., Okell, T.W., 2015. An optimized encoding scheme for planning vessel-encoded pseudocontinuous arterial spin labeling. Magn. Reson. Med. 74, 1248–1256.

Birn, R.M., Bandettini, P.A., Cox, R.W., Jesmanowicz, A., Shaker, R., 1998. Magnetic field changes in the human brain due to swallowing or speaking. Magn. Reson. Med. 40, 55–60.

Chen, Z., Zhao, X., Zhang, X., Guo, R., Teeuwisse, W.M., Zhang, B., Koken, P., Smink, J., Yuan, C., van Osch, M.J.P., 2018. Simultaneous measurement of brain perfusion and labeling efficiency in a single pseudo-continuous arterial spin labeling scan. Magn. Reson. Med. 79, 1922–1930.

Dai, W., Varma, G., Scheidegger, R., Alsop, D.C., 2016. Quantifying fluctuations of resting state networks using arterial spin labeling perfusion MRI. J. Cereb. Blood Flow Metab. 36, 463–473.

Gevers, S., Bokkers, R.P., Hendrikse, J., Majoie, C.B., Kies, D.A., Teeuwisse, W.M., Nederveen, A.J., van Osch, M.J., 2012. Robustness and reproducibility of flow territories defined by planning-free vessel-encoded pseudocontinuous arterial spin-labeling. AJNR Am. J. Neuroradiol. 33, E21–E25.

Gunther, M., 2006. Efficient visualization of vascular territories in the human brain by cycled arterial spin labeling MRI. Magn. Reson. Med. 56, 671–675.

Hartkamp, N.S., Bokkers, R.P.H., van der Worp, H.B., van Osch, M.J.P., Kappelle, L.J., Hendrikse, J., 2011. Distribution of cerebral blood flow in the caudate nucleus, lentiform nucleus and thalamus in patients with carotid artery stenosis. Eur. Radiol. 21, 875–881.

Hartkamp, N.S., Hendrikse, J., De Cocker, L.J.L., de Borst, G.J., Kappelle, L.J., Bokkers, R.P.H., 2016. Misinterpretation of Ischaemic Infarct Location in Relationship to the Cerebrovascular Territories. 87, 1084-1090.

Hendrikse, J., Petersen, E.T., Cheze, A., Chng, S.M., Venketasubramanian, N., Golay, X., 2009. Relation between cerebral perfusion territories and location of cerebral infarcts. Stroke 40, 1617–1622.

Hu, Y., Li, X., Wang, L., Han, B., Nie, S., 2020. T-distribution stochastic neighbor embedding for fine brain functional parcellation on rs-fMRI. Brain Res. Bull. 162, 199–207.

Hyvarinen, A., 1999. Fast and robust fixed-point algorithms for independent component analysis. IEEE Trans. Neural Netw. 10, 626–634.

Minka, T.P., 2000. Automatic Choice of Dimensionality for PCA. MIT Media Lab Vision and Modeling Group Technical Report 514.

Pezzotti, N., Höllt, T., Lelieveldt, B., Eisemann, E., Vilanova, A., 2016. Hierarchical Stochastic Neighbor Embedding. 35, 21-30.

Qiu, M., Paul Maguire, R., Arora, J., Planeta-Wilson, B., Weinzimmer, D., Wang, J., Wang, Y., Kim, H., Rajeevan, N., Huang, Y., Carson, R.E., Constable, R.T., 2010. Arterial transit time effects in pulsed arterial spin labeling CBF mapping: insight from a PET and MR study in normal human subjects. Magn. Reson. Med. 63, 374–384.

Raj, D., Anderson, A.W., Gore, J.C., 2001. Respiratory effects in human functional magnetic resonance imaging due to bulk susceptibility changes. Phys. Med. Biol. 46, 3331–3340.

Smith, S.M., 2002. Fast robust automated brain extraction. Hum. Brain Mapp. 17, 143–155.

van der Maaten, L., Hinton, G., 2008. Visualizing data using t-SNE. J. Mach. Learn. Res. 9, 2579–2605.

van Laar, P.J., van der Grond, J., Hendrikse, J., 2008. Brain perfusion territory imaging: methods and clinical applications of selective arterial spin-labeling MR imaging. Radiology 246, 354–364.

Verbree, J., van Osch, M.J.P., 2018. Influence of the cardiac cycle on pCASL: cardiac triggering of the end-of-labeling. Magma 31, 223–233.

Versluis, M.J., Sutton, B.P., de Bruin, P.W., Börnert, P., Webb, A.G., van Osch, M.J., 2012. Retrospective Image Correction in the Presence of Nonlinear Temporal Magnetic Field Changes Using Multichannel Navigator Echoes. 68, 1836-1845.

Wong, E.C., 2007. Vessel-encoded arterial spin-labeling using pseudocontinuous tagging. Magn. Reson. Med. 58, 1086–1091.

Wong, E.C., Guo, J., 2012. Blind detection of vascular sources and territories using random vessel encoded arterial spin labeling. Magn. Reson. Mater. Phys. Biol. Med. 25, 95–101.

Wu, W.-C., Jiang, S.-F., Yang, S.-C., Lien, S.-H., 2011. Pseudocontinuous arterial spin labeling perfusion magnetic resonance imaging—a normative study of reproducibility in the human brain. Neuroimage 56, 1244–1250.

Wu, W.C., Fernández-Seara, M., Detre, J.A., Wehrli, F.W., Wang, J., 2007. A theoretical and experimental investigation of the tagging efficiency of pseudocontinuous arterial spin labeling. Magn. Reson. Med. 58, 1020–1027.

Yerys, B.E., Herrington, J.D., Bartley, G.K., Liu, H.S., Detre, J.A., Schultz, R.T., 2018. Arterial spin labeling provides a reliable neurobiological marker of autism spectrum disorder. J. Neurodev. Disord. 10, 32.

Zhao, L., Vidorreta, M., Soman, S., Detre, J.A., Alsop, D.C., 2017. Improving the robustness of pseudo-continuous arterial spin labeling to off-resonance and pulsatile flow velocity. Magn. Reson. Med. 78, 1342–1351.

Zimine, I., Petersen, E.T., Golay, X., 2006. Dual vessel arterial spin labeling scheme for regional perfusion imaging. Magn. Reson. Med. 56, 1140–1144.